Between-Frequency Topographical and Dynamic High-Order Functional Connectivity for Driving Drowsiness Assessment

Jonathan Harvy, Nitish Thakor, *Fellow, IEEE*, Anastasios Bezerianos, *Senior Member, IEEE*, and Junhua Li, *Senior Member, IEEE*

***Abstract*— Previous studies exploring driving drowsiness utilized spectral power and functional connectivity without considering between-frequency and more complex synchronizations. To complement such lacks, we explored inter-regional synchronizations based on the topographical and dynamic properties between frequency bands using high-order functional connectivity (HOFC) and envelope correlation. We proposed the dynamic interactions of HOFC, associated-HOFC, and a global metric measuring the aggregated effect of the functional connectivity. The EEG dataset was collected from 30 healthy subjects, undergoing two driving sessions. The two-session setting was employed for evaluating the metric reliability across sessions. Based on the results, we observed reliably significant metric changes, mainly involving the alpha band. In HOFC$_{\theta\alpha}$, HOFC$_{\alpha\beta}$, associated-HOFC$_{\theta\alpha}$, and associated-HOFC$_{\alpha\beta}$, the connection-level metrics in frontal-central, central-central, and central-parietal/occipital areas were significantly increased, indicating a dominance in the central region. Similar results were also obtained in the HOFC$_{\theta\alpha\beta}$ and aHOFC$_{\theta\alpha\beta}$. For dynamic-low-order-FC and dynamic-HOFC, the global metrics revealed a reliably significant increment in the alpha, theta-alpha, and alpha-beta bands. Modularity indexes of associated-HOFC$_{\alpha}$ and associated-HOFC$_{\theta\alpha}$ also exhibited reliably significant differences. This paper demonstrated that within-band and between-frequency topographical and dynamic FC can provide complementary information to the traditional individual-band LOFC for assessing driving drowsiness.**

***Index Terms*— High-order functional connectivity, supra-adjacency matrix, dynamic connectivity, between-frequency connectivity, driving drowsiness, EEG.**

Manuscript received June 29, 2018; revised November 21, 2018; accepted January 3, 2019. Date of publication January 21, 2019; date of current version March 22, 2019. This work was supported in part by the National Natural Science Foundation of China under Grant 61806149, in part by the Ministry of Education of Singapore under Grant MOE2014-T2-1-115, and in part by the NUS Startup under Grant R-719-000-200-133. *(Corresponding author: Junhua Li.)*

J. Harvy, N. Thakor, and A. Bezerianos are with the Singapore Institute for Neurotechnology, National University of Singapore, Singapore 117456.

J. Li is with the Singapore Institute for Neurotechnology, National University of Singapore, Singapore 117456, also with the Laboratory for Brain-Bionic Intelligence and Computational Neuroscience, Wuyi University, Jiangmen 529020, China, and also with the Centre for Multidisciplinary Convergence Computing, School of Computer Science and Engineering, Northwestern Polytechnical University, Xi'an 710072, China (e-mail: juhalee.bcmi@gmail.com).

This paper has supplementary downloadable material available at http://ieeexplore.ieee.org, provided by the author.

Digital Object Identifier 10.1109/TNSRE.2019.2893949

I. Introduction

MENTAL fatigue is a cumulative process of vigilance decrement and is associated with a disinclination to any effort, leading to drowsiness and impaired performance [1], [2]. Although mental fatigue can be induced by a demanding cognitive activity [3], it can also be produced in a prolonged monotonous task, especially during driving [4]. Drivers in drowsiness state usually experience vigilance and performance decrements [2]. Accounting for 20% of all global traffic accidents, driving drowsiness is one of the prominent causes of traffic fatalities [5]. Due to the harmful repercussions of driving drowsiness, studies have been conducted to better understand its physiological process and to develop an effective countermeasure [1]. Physiological signals from brain (EEG), heart (ECG), and eye (EOG) have been utilized to indicate driving drowsiness [6]–[8]. Among these signals, EEG may be relatively reliable to indicate driving drowsiness since it directly reflects the brain activity, containing informative features associated with drowsiness [1], [9]–[11].

Previous studies have utilized spectral powers as indicators of driving drowsiness and mental fatigue [2], [12]–[15]. Spectral powers in typical frequency bands (i.e., theta, alpha, and beta) have been found to be closely related to driving drowsiness. Spectral powers in alpha and theta bands increased during heightened fatigue [2], [6], [8], [9], [13], [14]. In alpha band, almost all regions have been reported to have relevance to the changes of fatigue level, consisting of occipital [6], [8], [9], [13], [14], parietal [6], [9], [13], central [6], [9], [13], and temporal [6], [13] areas. Frontal [6], [13], [14], central and occipital [6], [13] regions in theta band were also found to be related to fatigue. In contrast, beta band significantly decreased during the state of driving drowsiness [6], [8], [9], which appeared in frontal [6], central [6], [9], and temporal [6] regions. A study using alpha spindle parameters also showed increases in spindle rate, duration, and amplitude during the period of drowsiness [12]. Spectral power ratio also showed significant differences between alertness and drowsiness. The ratios β/α and $(\alpha+\theta)/\beta$ decreased and increased respectively when becoming drowsy [2]. Delta and gamma bands were also reported to be associated with drowsiness [9], although they were much less frequently utilized compared to the theta, alpha, and beta bands in the published literature. The aforementioned

studies demonstrated that driving drowsiness is related to wide brain regions and particular frequency bands. These characteristics require the exploration of driving drowsiness from the perspective of inter-regional and between-frequency interactions, rather than from individually isolated brain regions.

In order to capture the inter-regional interactions, recent studies have utilized functional connectivity and the corresponding graph metrics to assess driving drowsiness and mental fatigue [16]–[24]. Significant increases of mean phase coherence (MPC) in delta and alpha bands were observed during the period of driving drowsiness and the number of connective functional units (FUs) also increased [16]. Studies using spectral coherence also showed similar results during heightened fatigue [18], [19]. Significant increases of coherence values were observed in delta, theta, alpha, and beta bands [18] and the number of synchronized regions also increased [19]. In a study using spectral coherence and phase locking value (PLV), significant increases of PLV values in theta band occurred after a prolonged cognitive task, while PLV and spectral coherence values in beta band decreased significantly [22]. Directed measures based on granger causality have also been utilized as fatigue indicators. A study using directed transfer function (DTF) revealed impaired parietal-to-frontal coupling in alpha band and enhanced frontal-to-center coupling in beta band in the left hemisphere [17]. Characteristic path length (L) and the normalized L computed from partial directed coherence in lower alpha band (8-10 Hz) increased significantly during fatigue, indicating an increasing inefficiency of information processing [21]. Such inefficiency during drowsiness was also observed in the delta and theta bands [20]. In a study using ordinary coherence [23], increases of the normalized clustering coefficient were observed in theta, alpha, and beta bands. Normalized L in theta and beta bands also increased under drowsiness [23]. As shown in the above studies, the dominant frequency bands (i.e., theta, alpha, and beta bands) involved in the connectivity were consistent with the frequency bands found in the spectral-power-based studies. Although these connectivity studies took inter-regional interactions into consideration, between-frequency interactions were neglected.

Since the brain functional connectivity in each frequency band has distinct information related to drowsiness, analyzing the connectivity between frequency bands may provide a more comprehensive view of driving drowsiness. Multilayer network has recently been developed to analyze multiple layers of brain functional connectivity in different bands by extracting their intralayer and interlayer interactions simultaneously [25]–[27]. In this study, we utilized the multilayer network which was previously utilized for schizophrenia studies [26], [27]. The networks within and between frequency bands were organized in a supra-adjacency matrix, consisting of the diagonal blocks representing the intralayer connectivity and the off-diagonal blocks representing the interlayer connectivity. To construct the supra-adjacency matrix, envelope correlation was utilized to measure the intrinsic mode of functional coupling within and between frequency bands [26], [27].

Although connectivity measures have been utilized as driving drowsiness indicators, they were considered as low-order functional connectivity (LOFC), ignoring the topographical and dynamic properties of the brain inter-regional interactions [28]–[30]. Functional connectivity utilizing the aforementioned properties may be more useful to assess driving drowsiness, capturing more complex inter-regional interactions. Recently, high-order functional connectivity (HOFC) has been proposed for fMRI data to capture high-order relationships between regions [28]–[32]. To capture the functional connectivity based on the topographical profiles, HOFC and associated HOFC (aHOFC) have been developed, characterizing the high level and inter level inter-regional synchronizations [32]. HOFC and aHOFC were collectively called as topographical FC (tFC) in this study. HOFC measures the similarity between pairs of LOFC profiles while aHOFC quantifies the relationship between LOFC and HOFC profiles. With the inspiration from the previous studies developing temporal correlation of LOFC [29], [30], we proposed the dynamic interactions of HOFC and aHOFC. This type of functional connectivity utilized the dynamic property of the connections, reflecting the adaptive and state-related temporary functional architecture of low level (dynamic LOFC, dLOFC), high level (dHOFC), and inter level (daHOFC) synchronizations respectively [29]. LOFC, HOFC, and aHOFC were collectively called as functional connectivity (FC) while dLOFC, dHOFC, and daHOFC were collectively called as dynamic FC (dFC) in this study.

In this paper, we proposed the use of topographical FC and dLOFC to characterize the brain functional connectivity in the alertness and drowsiness states. Based on the developed dLOFC, we proposed dHOFC and daHOFC to characterize the dynamic interactions of HOFC and aHOFC. We further proposed a global metric to measure the overall synchronization of FC and dFC during alertness and drowsiness. Connection-level metric and modularity index were calculated from the constructed FC and dFC, measuring inter-regional connections and the community structure respectively.

II. Methods

A. Experimental Protocol

All subjects, consisting of 30 healthy students, were recruited from the National University of Singapore (18 males and 12 females, age: 23.17 ± 2.72 years, mean $\pm$ standard deviation). All of them reported normal or corrected-to-normal vision. They had no history of substance addiction or mental disorders. The subjects were required to obtain a full night (>7 h) sleep before the day of the experiment and to refrain from consuming caffeine or alcohol on the day of the experiment. All subjects were trained to familiarize with the driving equipment and gave informed consent before the start of the experiment. The experiment was implemented with a driving simulation using Logitech G27 Racing Wheel set and Carnetsoft Driving Simulator (http://cs-driving-simulator.com) software. The subjects were required to steer a car following a guiding car, and to brake as soon as the red tail lights of the guiding car lit. Each subject completed two identical

90-minute driving sessions, approximately one week apart. The data from the two-session experiment were used for investigating the reliability of the metrics.

B. Data Acquisition

The brain activity was measured using EEG. EEG signals were recorded by the wireless dry 24-channel EEG system (Cognionics, Inc., USA), sampled at 250 Hz. The impedances of all EEG channels were maintained below 20 $K\Omega$ and referenced to the left and right mastoids. To obtain clean EEG epochs, several preprocessing steps were implemented. The EEG signals from all channels were first re-referenced using the common average reference. The signals from EEG channels having poor contact with the scalp were removed and interpolated using the ones from their adjacent channels. The last 5-min portion of EEG was removed due to the change of driving mode (i.e., free driving without the guiding car). The EEG signals were band-pass filtered using the FIR filter with 0.5 and 45 Hz cut-off frequencies. The filtered signals were then segmented into 2-second time epochs. Epoch rejection was performed using EEGLAB to remove abnormal epochs with more than 5 times standard deviation from the mean [33]. Due to an insufficient number of epochs after the rejection step, four subjects in the first session and one subject in the second session were excluded for further analysis. For the remaining subjects, the resulting epochs were decomposed into signal components using Independent Component Analysis (ICA). The components representing artifacts, such as eye movements, muscular activities, etc., were removed and the remaining components were used to reconstruct clean EEG epochs. The resulting epochs during the first and the last 5 minutes were considered as alertness (128.47 ± 21.44, mean $\pm$ standard deviation) and drowsiness (116.71 ± 31.73) samples, based on the self-reported confirmation from the subjects after the experiment and the increased reaction time at the end of the experiment relative to the beginning.

C. Low-Order FC by Envelope Correlation

The low-order FC was constructed by computing the envelope correlation of EEG signals. The signals in each epoch were band-pass filtered to theta (4-8 Hz), alpha (8-13 Hz), and beta (13-30 Hz) bands, which were frequently reported in the previous studies as relevant to drowsiness [17], [18], [20], [21], [23]. The envelopes of the filtered signals were computed using the Hilbert transform. The LOFC elements were then obtained by calculating the absolute Pearson's correlation of the envelopes, both for within and between frequency bands. The detailed steps for calculating the envelope correlation can be found in [26] and [27].

In order to concurrently consider the information contained in the individual frequency bands, supra-adjacency matrix was constructed to combine the information within and between frequency bands. In this study, individual-band and between-frequency FC and dFC were computed within and between theta, alpha, and beta bands. The between-frequency connectivity among the three bands resulted in theta-alpha, theta-beta, alpha-beta, and theta-alpha-beta matrices. The individual-band matrices have the dimension of 24×24 while the supra-adjacency matrices have the sizes of 48×48 (two bands) and 72×72 (three bands).

D. Topographical and Dynamic FC

Besides LOFC, we further extended our connectivity analysis to topographical FC and dynamic FC, exploring the inter-regional interactions based on different properties of synchronizations. HOFC and aHOFC were utilized to measure the topographical inter-regional synchronizations at high level and inter level respectively. The HOFC matrix was generated by computing the Pearson's correlation between any two columns of LOFC, each of which represents a region's topographical profile. Before performing the correlation, self-connections were removed and the elements were z-transformed. For the between-frequency HOFC, the resulting matrix consists of intralayer and interlayer blocks, in which the nodes in band x were denoted by intra$_x$-HOFC$_{xy}$ and inter$_x$-HOFC$_{xy}$ for the HOFC between band x and band y. Measuring the inter level interactions, aHOFC was constructed by computing the Pearson's correlation between the region's low level and high level topographical profiles. Since aHOFC contains elements of the synchronization between LOFC and HOFC, the LOFC/HOFC nodes in band x of the aHOFC between band x and band y were denoted by LOFC$_x$-aHOFC$_{xy}$/HOFC$_x$-aHOFC$_{xy}$. The steps for constructing topographical FC matrices were depicted in the top panel of Fig. 1, where the correlation of any two different columns (topographical profiles) resulted in a similarity value.

To characterize the between-connection interactions, dynamic FC was constructed, resulting in dLOFC, dHOFC, and daHOFC. This connectivity method calculates the Pearson's correlation between any two time series of each connection over the periods of alertness and drowsiness, resulting in a connectivity with a higher number of elements than the ones in the respective FC. The steps were depicted in the bottom panel of Fig. 1, where the resulting elements were computed from the correlation between the time series of any two different FC elements.

In this study, FC and dFC were utilized to capture the inter-regional interactions within and between theta, alpha, and beta bands. The resulting individual-band HOFC and aHOFC have the dimensions of 24×24, while the constructed between-frequency HOFC and aHOFC have the sizes of 48×48 (two bands) and 72×72 (three bands). The individual-band and between-frequency dLOFC and dHOFC have the sizes of 276×276 (one band), 1128×1128 (two bands), and 2556×2556 (three bands) while the sizes of daHOFC are 576×576 (one band), 2304×2304 (two bands), and 5184×5184 (three bands).

E. Global, Connection-Level Metrics and Modularity

To measure the overall synchronization of a connectivity matrix, we proposed a global metric which calculates the average value of the absolute unique elements in FC and

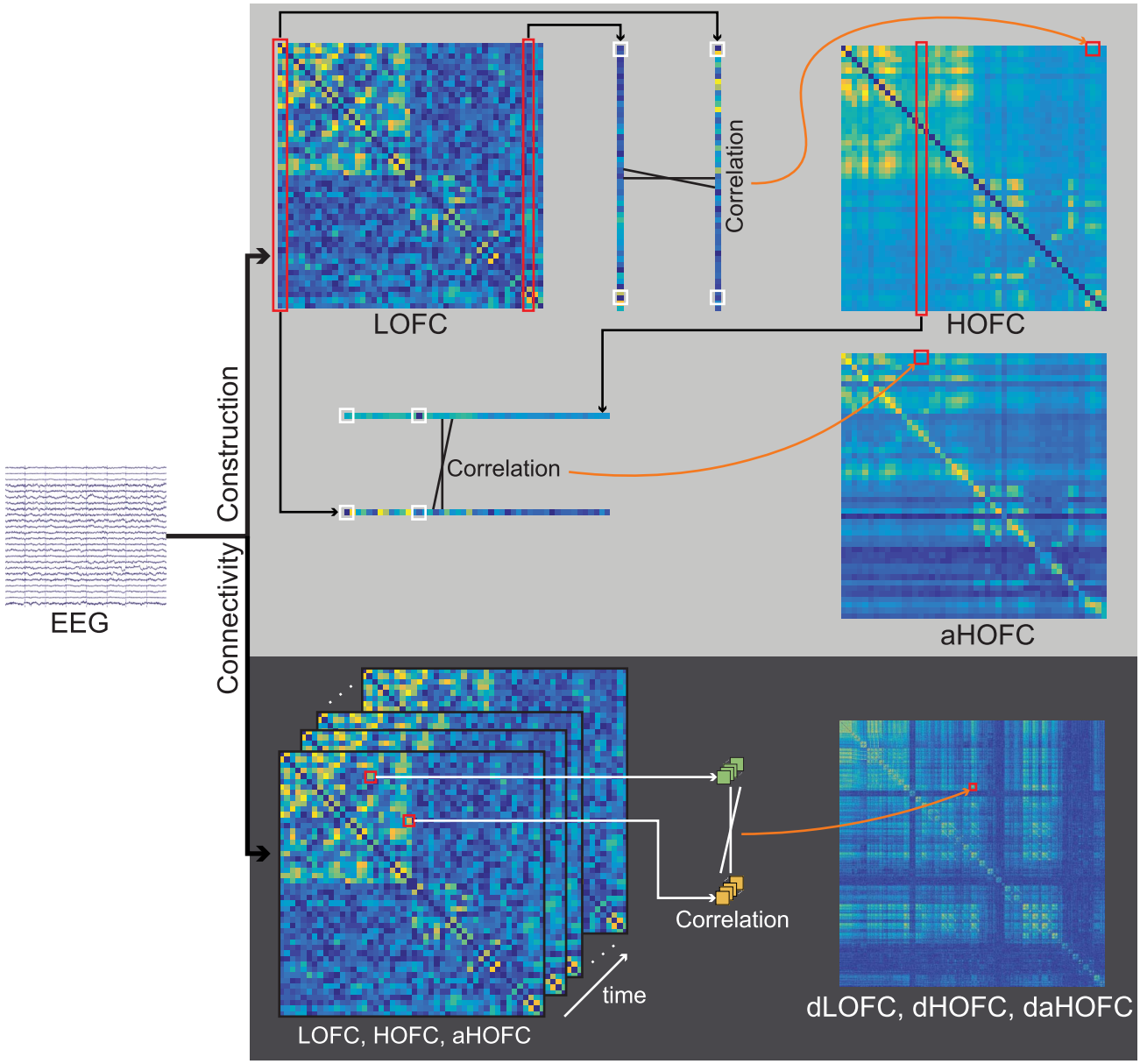

Fig. 1. An illustration of the construction of functional connectivity (FC) and dynamic FC (dFC) matrices. In the top panel, the elements of the HOFC matrix were obtained from computing the correlations between any two columns of the z-transformed LOFC matrix, excluding the self-connections shown in the white boxes. Similarly for aHOFC, the correlations were performed between the columns of LOFC and HOFC to calculate its elements. In the bottom panel, the time series of any two elements from FC matrix were correlated to compute each element of the dFC matrix.

dFC matrices. For symmetrical matrices of LOFC, HOFC, and dynamic FC, the global metric was calculated from the upper triangular elements of the connectivity matrix. For asymmetrical matrices of aHOFC, the global metric was computed from all elements of the matrix. Each element of the connectivity matrix was considered as the connection-level metric, quantifying the inter-regional connections of FC and dynamic FC. In addition to the global and connection-level metrics, modularity index was calculated for FC and dFC matrices to estimate the interconnection within communities relative to the one between communities [34].

Statistical analysis across subjects, using paired t-test, was performed on the global, connection-level metrics, and modularity indexes between the two states, separately for the first session and the second session. To minimize the possibility for the type I error of the connection-level metric, a false discovery rate (FDR) correction based on the Benjamini-Hochberg method was utilized. To focus on the reliable connection-level metrics, only the connections which were significant in both sessions after FDR correction were shown and discussed in this study.

III. Results

The overall synchronizations of LOFC during alertness and drowsiness were shown in Table I. In the individual-band and between-frequency LOFC, the overall synchronizations increased significantly in both sessions. Statistical analyses

TABLE I
THE GLOBAL METRICS OF LOFC DURING ALERTNESS AND DROWSINESS

Global Metrics		Alertness Mean (S.D.)	Drowsiness Mean (S.D.)	p-Value	t-Value
$LOFC_{\theta}$	Session 1	0.3988 (0.0522)	0.4076 (0.0557)	**0.03594**	-2.2170
	Session 2	0.4036 (0.0528)	0.4142 (0.0570)	**0.02404**	-2.3859
$LOFC_{\alpha}$	Session 1	0.3671 (0.0598)	0.3895 (0.0678)	**0.00044**	-4.0444
	Session 2	0.3806 (0.0617)	0.4005 (0.0588)	**0.00193**	-3.4211
$LOFC_{\beta}$	Session 1	0.2590 (0.0657)	0.2788 (0.0662)	**0.00045**	-4.0348
	Session 2	0.2706 (0.0712)	0.2874 (0.0740)	**0.02098**	-2.4462
$LOFC_{\theta\alpha}$	Session 1	0.3142 (0.0299)	0.3261 (0.0330)	**0.00015**	-4.4726
	Session 2	0.3207 (0.0315)	0.3308 (0.0317)	**0.00840**	-2.8354
$LOFC_{\theta\beta}$	Session 1	0.2356 (0.0298)	0.2461 (0.0311)	**0.00007**	-4.7549
	Session 2	0.2404 (0.0322)	0.2504 (0.0357)	**0.01088**	-2.7278
$LOFC_{\alpha\beta}$	Session 1	0.2283 (0.0334)	0.2435 (0.0366)	**0.00025**	-4.2606
	Session 2	0.2358 (0.0359)	0.2490 (0.0366)	**0.00385**	-3.1510

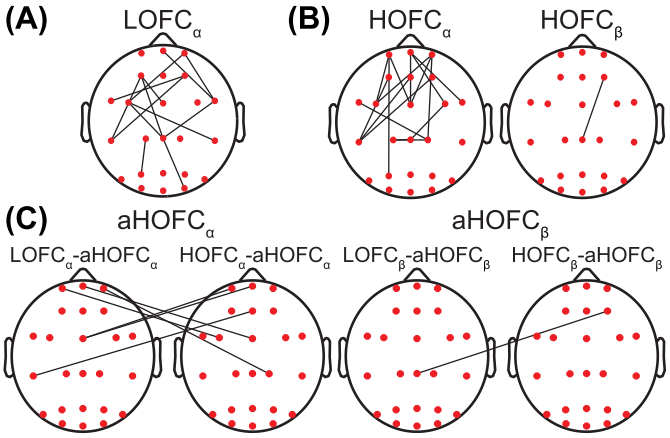

Fig. 2. Significant connection-level metrics of individual-band LOFC (A), HOFC (B), and aHOFC (C). The term LOFC$_{\alpha}$-aHOFC$_{\alpha}$ in this case refers to the LOFC in alpha band which is part of aHOFC$_{\alpha}$.

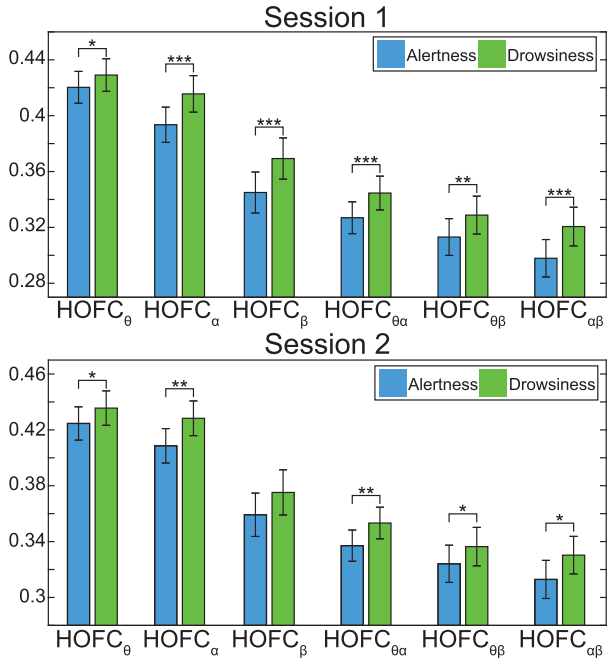

Fig. 3. Comparisons between alertness and drowsiness using the global metrics of HOFC (*: $p < 0.05$; **: $p < 0.01$; ***: $p < 0.001$).

of the connection-level metrics showed significant changes in both sessions only for LOFC$_{\alpha}$, depicted in Fig. 2(A).

The global metrics of HOFC during the two states were shown in Fig. 3. For individual-band HOFC, HOFC$_{\theta}$ and HOFC$_{\alpha}$ revealed significant increases of overall synchronization in both sessions, while a significant increase for HOFC$_{\beta}$ was found only in the first session. Observing the respective connection-level metrics, only HOFC$_{\alpha}$ and HOFC$_{\beta}$ showed significant changes in both sessions, depicted in Fig. 2(B). For between-frequency HOFC, HOFC$_{\theta\alpha}$, HOFC$_{\theta\beta}$, and HOFC$_{\alpha\beta}$ showed significant global metric increases during drowsiness in both sessions. Significant connection-level metric increases were found only for HOFC$_{\theta\alpha}$ (Fig. 4(A)) and HOFC$_{\alpha\beta}$ (Fig. 4(B)). Higher differences and number of significant connections were found involving the intra$_{\alpha}$-HOFC$_{\theta\alpha}$ and intra$_{\alpha}$-HOFC$_{\alpha\beta}$, represented in the matrix and connectivity plots. Significant increases of interlayer connections were also revealed, comprising notable frontal-central, central-central, and central-parietal/occipital connections.

The global metrics of aHOFC during alertness and drowsiness can be observed in Fig. 5. Significant increases in both sessions were found for aHOFC$_{\theta}$, aHOFC$_{\alpha}$, aHOFC$_{\beta}$, aHOFC$_{\theta\alpha}$, and aHOFC$_{\alpha\beta}$ while aHOFC$_{\theta\beta}$ showed a significant increase only in the first session. Based on the corresponding connection-level metrics, aHOFC$_{\alpha}$ and aHOFC$_{\beta}$ revealed significant connections as depicted in Fig. 2(C). In Fig. 6, the significant connection-level metrics of aHOFC$_{\theta\alpha}$ and aHOFC$_{\alpha\beta}$ were shown in the matrix and connectivity plots. In the matrix representations of Fig. 6(A) and Fig. 6(B), the significant connections, mainly involving LOFC$_{\alpha}$-aHOFC$_{\theta\alpha}$ and LOFC$_{\alpha}$-aHOFC$_{\alpha\beta}$, were scattered in a row-shaped fashion, indicating one low level topographical profile becoming more similar to several high level topographical profiles during drowsiness. Similar to the connection-level metrics of HOFC$_{\theta\alpha}$ and HOFC$_{\alpha\beta}$, notable interlayer connections mainly involving the central region were found for aHOFC$_{\theta\alpha}$ (Fig. 6(A)) and aHOFC$_{\alpha\beta}$ (Fig. 6(B)).

We further explored the degree of the significant connections, as shown in Fig. 4 and Fig. 6 (see Fig. 7). The degree plots, depicting the regional centralities, provided complementary information to the previous connectivity plots. Fig. 7(A) represented the degree plots of HOFC$_{\theta\alpha}$ and aHOFC$_{\theta\alpha}$. For HOFC$_{\theta\alpha}$, the nodes in the alpha band had higher degrees compared to the ones in the theta band, especially in the central region. For aHOFC$_{\theta\alpha}$, the nodes of the LOFC$_{\alpha}$-aHOFC$_{\theta\alpha}$ showed high degrees, mainly in the frontal-central and central-parietal areas. Fig. 7(B) depicted the degree plots of HOFC$_{\alpha\beta}$ and aHOFC$_{\alpha\beta}$. For HOFC$_{\alpha\beta}$, the nodes around the central region had high degrees and the highest was found in the central-parietal region. For aHOFC$_{\alpha\beta}$, the same nodes in the central-parietal region of LOFC$_{\alpha}$-aHOFC$_{\alpha\beta}$ and LOFC$_{\beta}$-aHOFC$_{\alpha\beta}$ had high degrees, revealing a high number of connections to/from that region.

The global metrics of dynamic FC were listed in Table II (dLOFC), Table III (dHOFC), and Table IV (daHOFC). In Table II, the global metrics of individual-band and between-frequency dLOFC revealed significant differences between

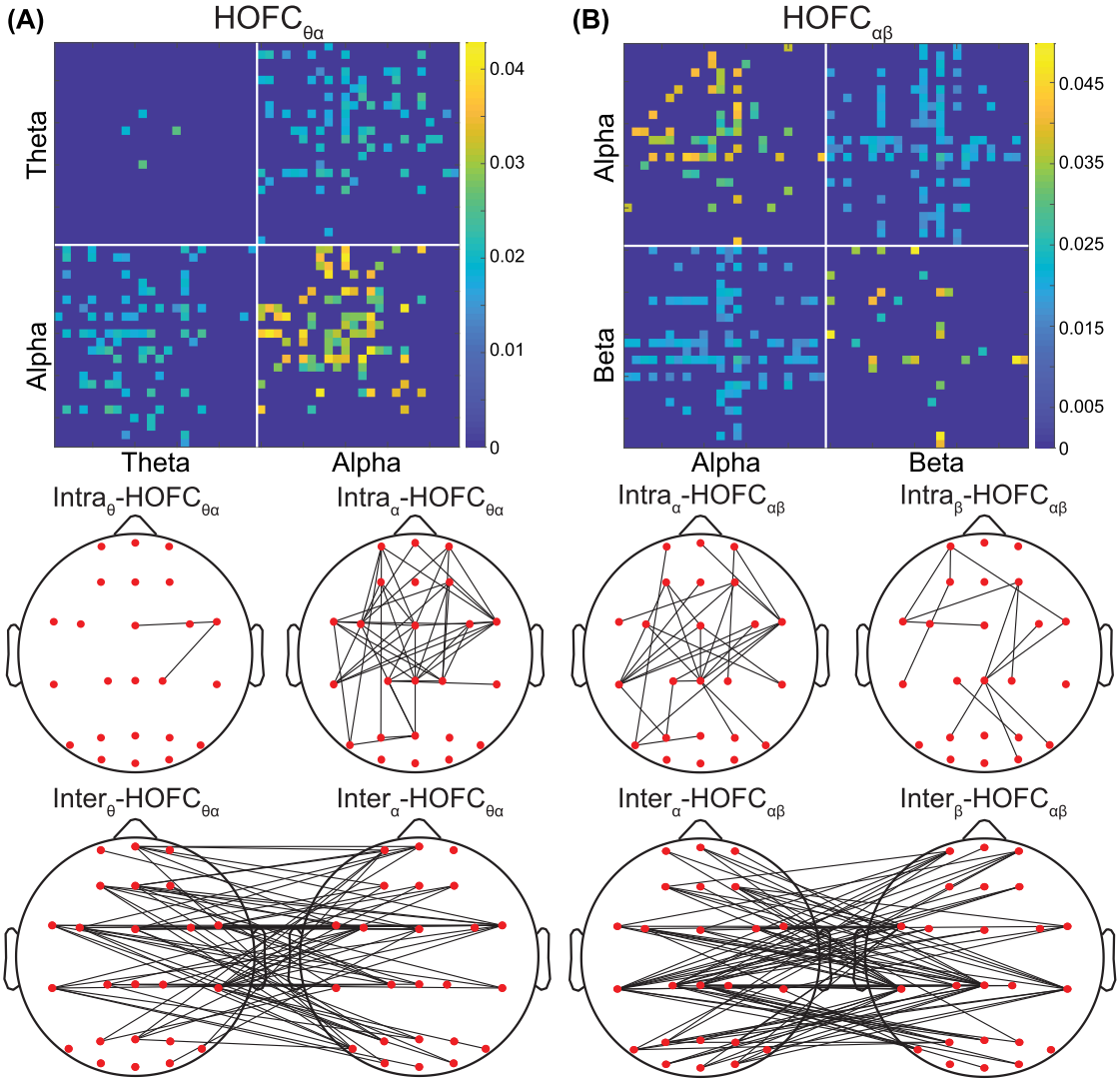

Fig. 4. Significant connection-level metrics of HOFC$_{\theta\alpha}$ (A) and HOFC$_{\alpha\beta}$ (B) in the matrix and connectivity plot representations. In the top panel, each colorbar represents the average value changes across the two sessions of the connection-level metrics during drowsiness relative to alertness. In the bottom panel, the term intra$_\theta$/inter$_\theta$-HOFC$_{\theta\alpha}$ refers to the nodes from the intralayer/interlayer blocks in theta band of the HOFC$_{\theta\alpha}$ matrix.

TABLE II
THE GLOBAL METRICS OF dLOFC DURING ALERTNESS AND DROWSINESS

Global Metric		Alertness Mean (S.D.)	Drowsiness Mean (S.D.)	p-Value	t-Value
dLOFC$_\theta$	Session 1	0.1308 (0.0349)	0.1420 (0.0377)	**0.01998**	-2.4856
	Session 2	0.1352(0.0387)	0.1467(0.0421)	0.12982	-1.5607
dLOFC$_\alpha$	Session 1	0.1392 (0.0404)	0.1732 (0.0667)	**0.00399**	-3.1706
	Session 2	0.1482 (0.0435)	0.1902 (0.0758)	**0.00385**	-3.1510
dLOFC$_\beta$	Session 1	0.1417 (0.0577)	0.1739 (0.0641)	**0.02336**	-2.4154
	Session 2	0.1505 (0.0564)	0.1849 (0.0685)	**0.01191**	-2.6898
dLOFC$_{\theta\alpha}$	Session 1	0.0931 (0.0163)	0.1069 (0.0248)	**0.00692**	-2.9433
	Session 2	0.0956 (0.0167)	0.1075 (0.0266)	**0.02281**	-2.4091
dLOFC$_{\theta\beta}$	Session 1	0.0918 (0.0221)	0.1055 (0.0267)	**0.03946**	-2.1731
	Session 2	0.0925 (0.0175)	0.1041 (0.0265)	0.05057	-2.0429
dLOFC$_{\alpha\beta}$	Session 1	0.0971 (0.0308)	0.1206 (0.0418)	**0.02911**	-2.3150
	Session 2	0.1031 (0.0307)	0.1264 (0.0443)	**0.00818**	-2.8465

TABLE III
THE GLOBAL METRICS OF dHOFC DURING ALERTNESS AND DROWSINESS

Global Metric		Alertness Mean (S.D.)	Drowsiness Mean (S.D.)	p-Value	t-Value
dHOFC$_\theta$	Session 1	0.1292 (0.0248)	0.1392 (0.0252)	0.08113	-1.8176
	Session 2	0.1360 (0.0317)	0.1408 (0.0288)	0.44573	-0.7735
dHOFC$_\alpha$	Session 1	0.1276 (0.0224)	0.1525 (0.0443)	**0.00248**	-3.3644
	Session 2	0.1426 (0.0288)	0.1615 (0.0451)	**0.03051**	-2.2787
dHOFC$_\beta$	Session 1	0.1255 (0.0308)	0.1487 (0.0343)	**0.00115**	-3.6690
	Session 2	0.1331 (0.0366)	0.1481 (0.0454)	0.07221	-1.8683
dHOFC$_{\theta\alpha}$	Session 1	0.1068 (0.0170)	0.1261 (0.0277)	**0.00047**	-4.0170
	Session 2	0.1140 (0.0224)	0.1289 (0.0318)	**0.03714**	-2.1884
dHOFC$_{\theta\beta}$	Session 1	0.1115 (0.0225)	0.1273 (0.0276)	**0.00443**	-3.1281
	Session 2	0.1183 (0.0260)	0.1302 (0.0303)	0.07854	-1.8259
dHOFC$_{\alpha\beta}$	Session 1	0.1129 (0.0229)	0.1330 (0.0322)	**0.00135**	-3.6059
	Session 2	0.1188 (0.0253)	0.1373 (0.0339)	**0.01078**	-2.7320

alertness and drowsiness in both sessions, except for the second session of dLOFC$_\theta$ and dLOFC$_{\theta\beta}$. In Table III, significant increases were shown during drowsiness in both sessions for dHOFC$_\alpha$, dHOFC$_{\theta\alpha}$, and dHOFC$_{\alpha\beta}$. The first session of dHOFC$_\beta$ and dHOFC$_{\theta\beta}$ showed significant changes while there were no significant differences in both sessions for dHOFC$_\theta$. Observing the overall synchronization changes of daHOFC in Table IV, we found that only daHOFC$_\theta$,

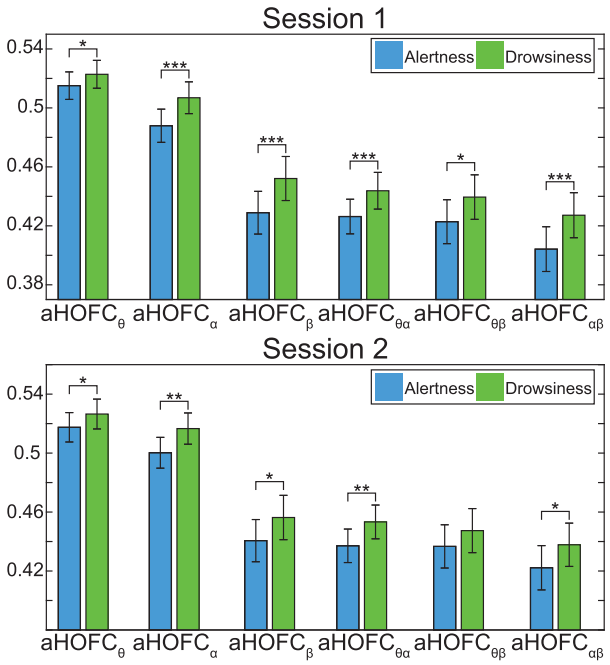

Fig. 5. Comparisons between alertness and drowsiness using the global metrics of aHOFC (*: $p < 0.05$; **: $p < 0.01$; ***: $p < 0.001$).

TABLE IV
THE GLOBAL METRICS OF DAHOFC DURING ALERTNESS AND DROWSINESS

Global Metric		Alertness Mean (S.D.)	Drowsiness Mean (S.D.)	p-Value	t-Value
daHOFC$_\theta$	Session 1	0.0982 (0.0121)	0.1111 (0.0262)	**0.01679**	-2.5627
	Session 2	0.1070 (0.0385)	0.1054 (0.0162)	0.82838	0.2188
daHOFC$_\alpha$	Session 1	0.0986 (0.0129)	0.1117 (0.0263)	**0.01663**	-2.5670
	Session 2	0.1082 (0.0360)	0.1062 (0.0164)	0.77493	0.2887
daHOFC$_\beta$	Session 1	0.1106 (0.0256)	0.1268 (0.0402)	0.05302	-2.0310
	Session 2	0.1301 (0.0722)	0.1201 (0.0252)	0.48030	0.7154
daHOFC$_{\theta\alpha}$	Session 1	0.0970 (0.0128)	0.1115 (0.0304)	**0.02121**	-2.4587
	Session 2	0.1076 (0.0412)	0.1065 (0.0194)	0.89704	0.1306
daHOFC$_{\theta\beta}$	Session 1	0.1157 (0.0170)	0.1318 (0.0449)	0.08611	-1.7868
	Session 2	0.1323 (0.0627)	0.1267 (0.0262)	0.65340	0.4539
daHOFC$_{\alpha\beta}$	Session 1	0.1128 (0.0181)	0.1298 (0.0379)	**0.02998**	-2.3014
	Session 2	0.1302 (0.0620)	0.1258 (0.0263)	0.72794	0.3514

daHOFC$_\alpha$, daHOFC$_{\theta\alpha}$, and daHOFC$_{\alpha\beta}$ in the first session revealed significant increases. After obtaining the connection-level metrics of the individual-band and between-frequency dynamic FC, we found no consistently significant changes.

The modularity indexes of FC and dynamic FC during alertness and drowsiness were shown in Table V and VI respectively. The modularity indexes of FC showed significant changes in both sessions for aHOFC$_\alpha$ and aHOFC$_{\theta\alpha}$. The first session of LOFC$_\beta$, HOFC$_\alpha$, HOFC$_\beta$, and aHOFC$_\beta$ also showed significant differences, while a significant change was found in the second session of HOFC$_{\theta\alpha}$. For the modularity of dynamic FC, significant differences were found only for dLOFC$_{\theta\beta}$ in the second session and dHOFC$_\alpha$ in the first session.

Between-frequency FC and dFC in theta-alpha-beta were also investigated, as shown in Table VII for the global metrics and in Fig. 8 for the connection-level metrics. For the global metrics, significant increases were found in both sessions, except for daHOFC$_{\theta\alpha\beta}$ in the second session. Significant changes in the connection-level metrics were observed for

TABLE V
THE MODULARITY OF FC DURING ALERTNESS AND DROWSINESS

Modularity		Alertness Mean (S.D.)	Drowsiness Mean (S.D.)	p-Value	t-Value
LOFC$_\theta$	Session 1	0.1140 (0.0162)	0.1122 (0.0188)	0.33149	0.9903
	Session 2	0.1081 (0.0183)	0.1084 (0.0195)	0.91532	-0.1073
LOFC$_\alpha$	Session 1	0.1168 (0.0162)	0.1124 (0.0227)	0.07619	1.8499
	Session 2	0.1106 (0.0187)	0.1080 (0.0191)	0.26881	1.1282
LOFC$_\beta$	Session 1	0.1363 (0.0218)	0.1268 (0.0296)	**0.02193**	2.4439
	Session 2	0.1272 (0.0307)	0.1262 (0.0300)	0.79303	0.2649
LOFC$_{\theta\alpha}$	Session 1	0.1548 (0.0163)	0.1559 (0.0178)	0.36035	-0.9318
	Session 2	0.1550 (0.0174)	0.1565 (0.0179)	0.28373	-1.0930
LOFC$_{\theta\beta}$	Session 1	0.1938 (0.0299)	0.1958 (0.0301)	0.33559	-0.9818
	Session 2	0.1962 (0.0295)	0.1963 (0.0287)	0.92238	-0.0983
LOFC$_{\alpha\beta}$	Session 1	0.1875 (0.0308)	0.1889 (0.0307)	0.56948	-0.5764
	Session 2	0.1911 (0.0295)	0.1909 (0.0308)	0.89594	0.1320
HOFC$_\theta$	Session 1	0.1060 (0.0106)	0.1052 (0.0113)	0.53799	0.6244
	Session 2	0.1029 (0.0134)	0.1027 (0.0148)	0.85135	0.1891
HOFC$_\alpha$	Session 1	0.1111 (0.0093)	0.1072 (0.0113)	**0.03644**	2.2105
	Session 2	0.1068 (0.0137)	0.1038 (0.0151)	0.09402	1.7335
HOFC$_\beta$	Session 1	0.1216 (0.0189)	0.1130 (0.0185)	**0.00022**	4.3229
	Session 2	0.1149 (0.0245)	0.1158 (0.0260)	0.80381	-0.2508
HOFC$_{\theta\alpha}$	Session 1	0.1315 (0.0066)	0.1302 (0.0078)	0.17085	1.4100
	Session 2	0.1301 (0.0052)	0.1281 (0.0065)	**0.04432**	2.1058
HOFC$_{\theta\beta}$	Session 1	0.1433 (0.0128)	0.1433 (0.0151)	0.98006	0.0252
	Session 2	0.1411 (0.0109)	0.1414 (0.0105)	0.85151	-0.1889
HOFC$_{\alpha\beta}$	Session 1	0.1457 (0.0117)	0.1440 (0.0151)	0.26829	1.1322
	Session 2	0.1444 (0.0109)	0.1429 (0.0112)	0.32961	0.9922
aHOFC$_\theta$	Session 1	0.1176 (0.0113)	0.1158 (0.0131)	0.26857	1.1315
	Session 2	0.1162 (0.0141)	0.1150 (0.0158)	0.45626	0.7555
aHOFC$_\alpha$	Session 1	0.1232 (0.0120)	0.1180 (0.0116)	**0.00195**	3.4593
	Session 2	0.1194 (0.0144)	0.1160 (0.0164)	**0.04935**	2.0546
aHOFC$_\beta$	Session 1	0.1333 (0.0231)	0.1246 (0.0239)	**0.00203**	3.4451
	Session 2	0.1276 (0.0248)	0.1260 (0.0255)	0.59370	0.5397
aHOFC$_{\theta\alpha}$	Session 1	0.1282 (0.0134)	0.1250 (0.0156)	**0.03375**	2.2465
	Session 2	0.1255 (0.0131)	0.1218 (0.0139)	**0.02063**	2.4535
aHOFC$_{\theta\beta}$	Session 1	0.1213 (0.0218)	0.1188 (0.0242)	0.39067	0.8736
	Session 2	0.1154 (0.0220)	0.1168 (0.0217)	0.53957	-0.6211
aHOFC$_{\alpha\beta}$	Session 1	0.1261 (0.0206)	0.1226 (0.0232)	0.18022	1.3786
	Session 2	0.1208 (0.0223)	0.1201 (0.0223)	0.81517	0.2360

HOFC$_{\theta\alpha\beta}$ and aHOFC$_{\theta\alpha\beta}$ (see Fig. 8), while none were found for LOFC$_{\theta\alpha\beta}$. Similar to the results in Fig. 7, the connections mostly involved the central region in the alpha band. The degree plots of HOFC$_{\theta\alpha\beta}$ and aHOFC$_{\theta\alpha\beta}$ were shown in the supplementary materials.

For the readers who are interested in the individual-band and between-frequency FC and dFC involving delta and gamma, we explored the respective global and connection-level metrics. In summary, we found similar results to the ones within and between theta, alpha, beta. Observing the global metrics of individual-band FC, we found reliably significant increases for LOFC$_\delta$, LOFC$_\gamma$, HOFC$_\delta$, and aHOFC$_\delta$. For the between-frequency tFC, we observed the dominance of the central region in alpha band for HOFC$_{\delta\alpha}$, HOFC$_{\alpha\gamma}$, and aHOFC$_{\alpha\gamma}$. Reliable global metrics of dynamic FC were found for dLOFC$_\gamma$, dLOFC$_{\delta\alpha}$, dLOFC$_{\alpha\gamma}$, and dHOFC$_{\alpha\gamma}$. The dominant central regions in alpha band were also revealed in the five-band FC. More details of the results were reported in the supplementary materials.

IV. DISCUSSION

A. Increasing Synchronization During Drowsiness

Based on the results of the statistical analyses, the global and connection-level metrics of FC and dynamic FC were increased during driving drowsiness. For the overall synchronization, reliable changes were found for within- and between-frequency FC and dFC. Previous connectivity studies also showed heightened synchronizations during drowsiness. In terms of the overall connectivity changes, increases of the

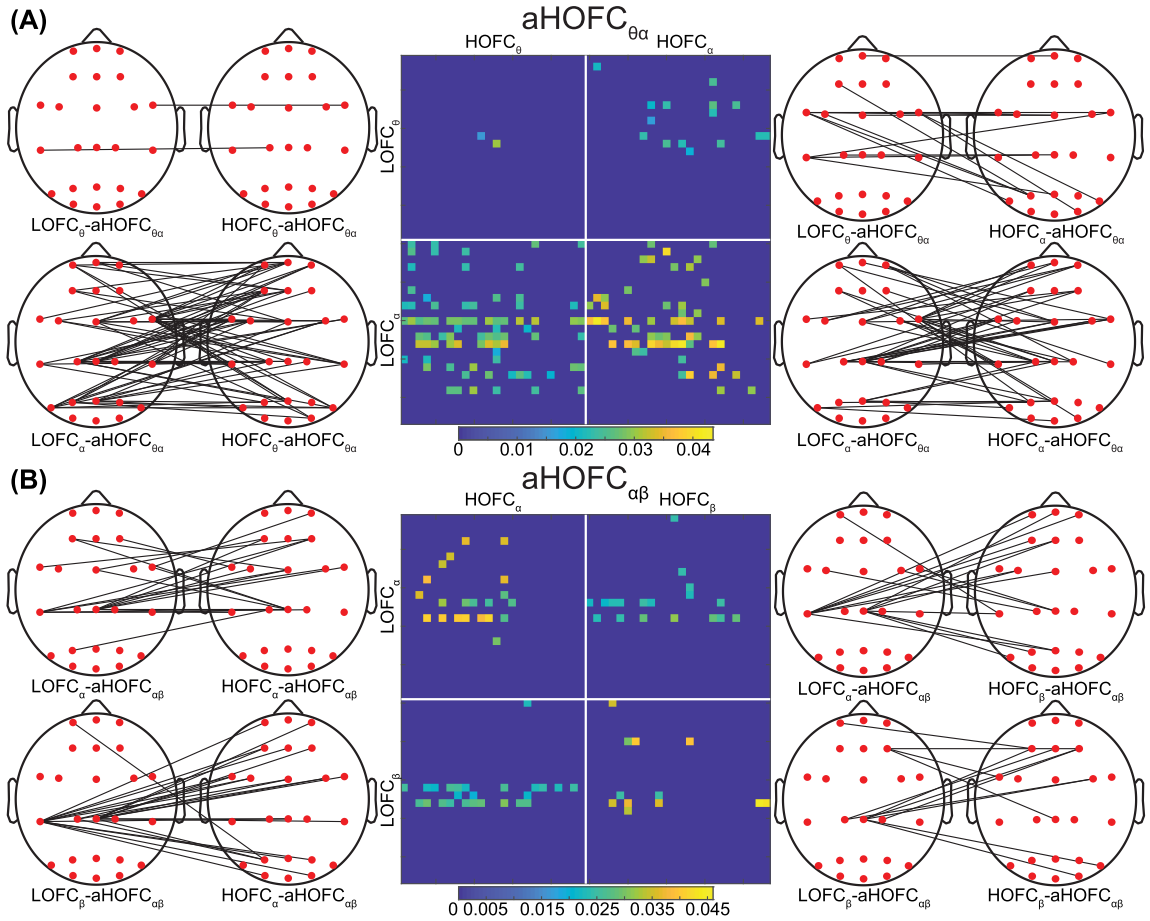

Fig. 6. Significant connection-level metrics of aHOFC$_{\theta\alpha}$ (A) and aHOFC$_{\alpha\beta}$ (B) in matrix and connectivity plot representations. Each colorbar represents the average value changes across the two sessions of the connection-level metrics during drowsiness relative to alertness. The term LOFC$_\theta$/HOFC$_\theta$-aHOFC$_{\theta\alpha}$ indicates the LOFC$_\theta$/HOFC$_\theta$ nodes of the aHOFC$_{\theta\alpha}$ matrix.

number of synchronized regions at higher level of drowsiness were found in theta, alpha, and beta bands [16]. Observing the connection-level metrics, we found consistently significant increases within and between-frequency HOFC and aHOFC. Stronger interactions of the central-parietal/occipital and frontal-central connections were found in HOFC$_{\theta\alpha}$, HOFC$_{\alpha\beta}$, HOFC$_{\theta\alpha\beta}$ and aHOFC$_{\theta\alpha}$, aHOFC$_{\alpha\beta}$, aHOFC$_{\theta\alpha\beta}$. In the previous connectivity studies, frontal-to-center DTF connections enhanced in beta band [17], while higher spectral granger causality values were observed in theta and alpha bands [20]. Parietal-occipital connective FUs were also found in theta, alpha, and beta bands during drowsiness period [16]. In conclusion, the results of the global and connection-level metrics were in agreement with the findings in the previous studies regarding the increasing inter-regional synchronizations during drowsiness. This observation might suggest that similar increases of synchronization during drowsiness at individual-band LOFC are also replicated at the individual-band and between-frequency topographical and dynamic FC.

B. Alpha Band Dominance During Drowsiness

From the previously mentioned bands related to driving drowsiness, the changes in alpha band were dominant in our study compared to that in theta and beta bands. According to the LOFC results, only LOFC$_\alpha$ had consistently significant differences of connection-level metrics, as shown in Fig. 2. Based on the toporaphical FC results, HOFC$_\alpha$, HOFC$_{\theta\alpha}$, HOFC$_{\alpha\beta}$, HOFC$_{\theta\alpha\beta}$ and aHOFC$_\alpha$, aHOFC$_{\theta\alpha}$, aHOFC$_{\alpha\beta}$, aHOFC$_{\theta\alpha\beta}$ showed reliable changes of global and connection-level metrics. In Fig. 4, the connections involving intra$_\alpha$-HOFC$_{\theta\alpha}$ and intra$_\alpha$-HOFC$_{\alpha\beta}$ had higher differences compared to the other reliable connections. Similar results were observed in aHOFC as shown in Fig. 6, mainly involving LOFC$_\alpha$-aHOFC$_{\theta\alpha}$ and LOFC$_\alpha$-aHOFC$_{\alpha\beta}$. In the connection-level metrics of HOFC$_{\theta\alpha\beta}$ and aHOFC$_{\theta\alpha\beta}$, the connections having significant changes were found mostly involving the alpha band (see Fig. 8). Based on the dynamic FC results, we found reliably significant increases of the global metrics of dLOFC$_\alpha$, dLOFC$_{\theta\alpha}$, dLOFC$_{\alpha\beta}$, dLOFC$_{\theta\alpha\beta}$ and dHOFC$_\alpha$, dHOFC$_{\theta\alpha}$, dHOFC$_{\alpha\beta}$, dHOFC$_{\theta\alpha\beta}$. The modularity indexes of aHOFC$_\alpha$ and aHOFC$_{\theta\alpha}$ also showed significant differences in both sessions. The observation of dominant alpha band changes during drowsiness was in concordance with the previous results using spectral power [2], [6], [9], [13] and functional connectivity [16]–[18], [20], [23]. Our findings in this study support the hypothesis that alpha band is dominant during relaxed conditions, decreased attention levels, and drowsy but wakeful state [6], [8].

TABLE VI
THE MODULARITY OF DFC DURING ALERTNESS AND DROWSINESS

Modularity		Alertness Mean (S.D.)	Drowsiness Mean (S.D.)	p-Value	t-Value
$dLOFC_{\theta}$	Session 1	0.1497 (0.0289)	0.1480 (0.0326)	0.72601	0.3544
	Session 2	0.1507 (0.0323)	0.1460 (0.0293)	0.30582	1.0431
$dLOFC_{\alpha}$	Session 1	0.1413 (0.0377)	0.1324 (0.0340)	0.11998	1.6099
	Session 2	0.1453 (0.0302)	0.1331 (0.0434)	0.09761	1.7138
$dLOFC_{\beta}$	Session 1	0.1361 (0.0344)	0.1348 (0.0273)	0.84604	0.1962
	Session 2	0.1368 (0.0259)	0.1280 (0.0300)	0.10426	1.6791
$dLOFC_{\theta\alpha}$	Session 1	0.1072 (0.0497)	0.1123 (0.0516)	0.38345	-0.8872
	Session 2	0.1179 (0.0526)	0.1271 (0.0486)	0.12730	-1.5715
$dLOFC_{\theta\beta}$	Session 1	0.1029 (0.0559)	0.1096 (0.0513)	0.22811	-1.2355
	Session 2	0.1090 (0.0517)	0.1214 (0.0517)	**0.01630**	-2.5562
$dLOFC_{\alpha\beta}$	Session 1	0.1003 (0.0533)	0.1068 (0.0457)	0.29351	-1.0730
	Session 2	0.1051 (0.0453)	0.1103 (0.0413)	0.17624	-1.3875
$dHOFC_{\theta}$	Session 1	0.1436 (0.0322)	0.1383 (0.0304)	0.33547	0.9821
	Session 2	0.1375 (0.0275)	0.1379 (0.0273)	0.92599	-0.0937
$dHOFC_{\alpha}$	Session 1	0.1416 (0.0325)	0.1330 (0.0366)	**0.04269**	2.1357
	Session 2	0.1387 (0.0279)	0.1356 (0.0383)	0.58610	0.5509
$dHOFC_{\beta}$	Session 1	0.1512 (0.0374)	0.1495 (0.0307)	0.73206	0.3462
	Session 2	0.1534 (0.0261)	0.1487 (0.0320)	0.36246	0.9258
$dHOFC_{\theta\alpha}$	Session 1	0.1061 (0.0321)	0.1054 (0.0297)	0.85127	0.1894
	Session 2	0.1103 (0.0345)	0.1081 (0.0276)	0.51021	0.6670
$dHOFC_{\theta\beta}$	Session 1	0.1195 (0.0337)	0.1210 (0.0361)	0.72644	-0.3538
	Session 2	0.1244 (0.0409)	0.1274 (0.0389)	0.51624	-0.6575
$dHOFC_{\alpha\beta}$	Session 1	0.1164 (0.0349)	0.1223 (0.0329)	0.15028	-1.4841
	Session 2	0.1242 (0.0408)	0.1295 (0.0442)	0.16000	-1.4434
$daHOFC_{\theta}$	Session 1	0.0642 (0.0235)	0.0678 (0.0272)	0.42235	-0.8157
	Session 2	0.0615 (0.0189)	0.0695 (0.0221)	0.13784	-1.5276
$daHOFC_{\alpha}$	Session 1	0.0681 (0.0286)	0.0709 (0.0277)	0.60528	-0.5234
	Session 2	0.0653 (0.0210)	0.0721 (0.0245)	0.24421	-1.1896
$daHOFC_{\beta}$	Session 1	0.0996 (0.0484)	0.1039 (0.0562)	0.70542	-0.3824
	Session 2	0.0975 (0.0395)	0.1079 (0.0492)	0.38736	-0.8781
$daHOFC_{\theta\alpha}$	Session 1	0.0683 (0.0259)	0.0705 (0.0278)	0.64280	-0.4695
	Session 2	0.0678 (0.0248)	0.0756 (0.0316)	0.23517	-1.2133
$daHOFC_{\theta\beta}$	Session 1	0.0976 (0.0343)	0.1009 (0.0443)	0.69484	-0.3969
	Session 2	0.0952 (0.0334)	0.1035 (0.0453)	0.42729	-0.8055
$daHOFC_{\alpha\beta}$	Session 1	0.0972 (0.0373)	0.1024 (0.0445)	0.53731	-0.6255
	Session 2	0.0946 (0.0369)	0.1030 (0.0459)	0.41145	-0.8338

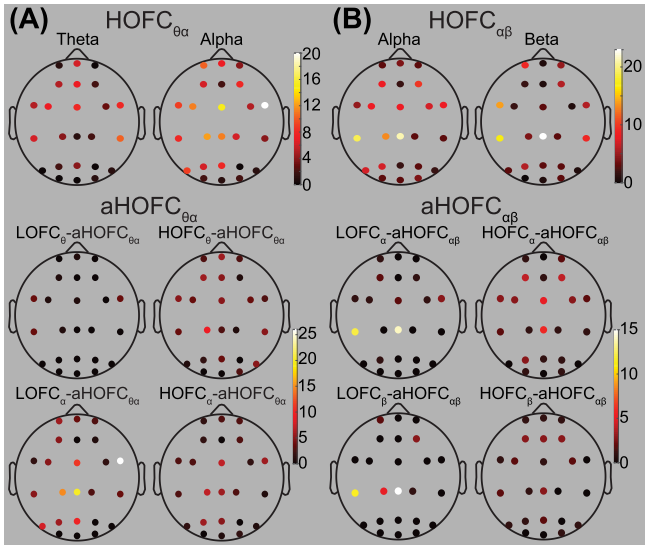

Fig. 7. Significant connection-level metrics of $HOFC_{\theta\alpha}$, $aHOFC_{\theta\alpha}$ (A) and $HOFC_{\alpha\beta}$, $aHOFC_{\alpha\beta}$ (B) in degree plot representation. The colorbars represent the respective degree values of the nodes. For HOFC, each headplot corresponds to the nodes from each band. For aHOFC, each headplot refers to the LOFC/HOFC nodes of the aHOFC.

C. Reliable Connections of Between-Frequency tFC Involving the Central Region

Most of the reliable connection-level metrics were found by utilizing the inter level (aHOFC) and high level (HOFC) topographical synchronizations. While only $LOFC_{\alpha}$ showed consistently significant changes of the connection-level metrics (Fig. 2(A)), more reliable metrics were observed in HOFC (Fig. 2(B)) and aHOFC (Fig. 2(C)). Further integrating the inter-regional interactions in several frequency bands, we found a higher number of reliable connection-level metrics of $HOFC_{\theta\alpha}$, $HOFC_{\alpha\beta}$ and $aHOFC_{\theta\alpha}$, $aHOFC_{\alpha\beta}$, as shown in Fig. 4 and Fig. 6. Observing the parts of the two-band HOFC, we found a high number of reliable connection-level metrics in the respective interlayer blocks, comprising central-central, frontal-central, and central-parietal/occipital connections. In two-band aHOFC, we also observed reliable changes of connection-level metrics in similar regions to the ones of HOFC. Central-central and frontal-central connections were also found in $HOFC_{\theta\alpha\beta}$ and $aHOFC_{\theta\alpha\beta}$. Previous LOFC studies also revealed enhanced frontal-central [17], [22] and central-central [22] connections during drowsiness. Further analyzing the respective degree plots, we found that the reliable connections mainly involved the central region as depicted in Fig. 7. Previous spectral power studies reported significant changes in central regions in theta [13], alpha [9], [13], and beta [9] bands during driving drowsiness. Similarly in the previous connectivity studies, higher mean MPC [16] and mean coherence [23] in the central region were also reported. In this study, between-frequency inter-regional connections, mainly involving the central region, exhibited more reliable changes at the inter level and high level synchronizations for drowsiness assessment. In addition, between-frequency topographical FC

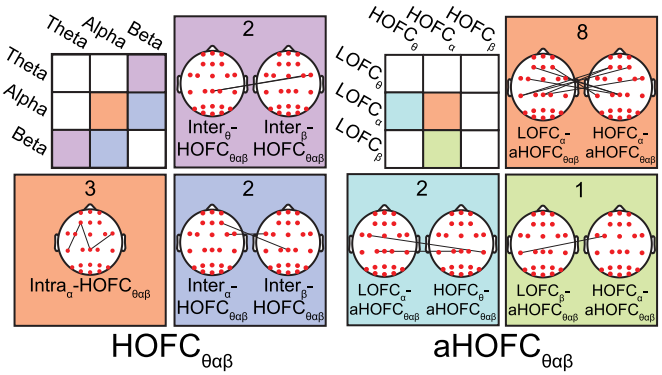

Fig. 8. Significant connection-level metrics of $HOFC_{\theta\alpha\beta}$ and $aHOFC_{\theta\alpha\beta}$.

TABLE VII
THE GLOBAL METRICS OF FC AND DFC IN THETA-ALPHA-BETA DURING ALERTNESS AND DROWSINESS

Global Metric		Alertness Mean (S.D.)	Drowsiness Mean (S.D.)	p-Value	t-Value
$LOFC_{\theta\alpha\beta}$	Session 1	0.2327 (0.0223)	0.2438 (0.0245)	**0.00007**	-4.7615
	Session 2	0.2378 (0.0240)	0.2474 (0.0261)	**0.00707**	-2.9064
$HOFC_{\theta\alpha\beta}$	Session 1	0.2595 (0.0491)	0.2764 (0.0510)	**0.00024**	-4.2754
	Session 2	0.2698 (0.0522)	0.2830 (0.0518)	**0.01287**	-2.6570
$aHOFC_{\theta\alpha\beta}$	Session 1	0.3484 (0.0537)	0.3655 (0.0541)	**0.00078**	-3.8229
	Session 2	0.3604 (0.0555)	0.3726 (0.0534)	**0.02350**	-2.3961
$dLOFC_{\theta\alpha\beta}$	Session 1	0.0856 (0.0201	0.0993 (0.0256)	**0.04137**	-2.1506
	Session 2	0.0869 (0.0146)	0.0983 (0.0248)	**0.03368**	-2.2336
$dHOFC_{\theta\alpha\beta}$	Session 1	0.0948 (0.0142)	0.1119 (0.0246)	**0.00200**	-3.4499
	Session 2	0.0992 (0.0166)	0.1134 (0.0273)	**0.02425**	-2.3820
$daHOFC_{\theta\alpha\beta}$	Session 1	0.1083 (0.0165)	0.1236 (0.0325)	**0.01740**	-2.5471
	Session 2	0.1193 (0.0446)	0.1204 (0.0250)	0.89793	-0.1294

may manifest the characteristics which cannot be captured by the individual-band LOFC.

V. Conclusion

In this paper, we utilized FC and dLOFC and proposed dHOFC and daHOFC within and between frequency bands to assess driving drowsiness. In addition to the connection-level metric and modularity, we proposed a global metric to measure the aggregated effect of FC and dynamic FC matrices. According to the LOFC results, the global metrics showed consistently significant increases within and between frequency bands while only LOFC_α revealed reliable changes of the connection-level metrics. By using between-frequency topographical FC, most of the reliable connection-level metrics were found, mainly involving the central region in the alpha band. Alpha band dominance was also observed in the global metrics of dynamic FC and modularity indexes of FC. In summary, the study suggested that between-frequency tFC is more sensitive than traditional within-band LOFC for assessing driving drowsiness. While the overall changes of LOFC were consistently significant, the use of between-frequency tFC could reveal reliably significant changes of overall synchronizations and a higher number of inter-regional connections. Reliable overall changes of individual-band and between-frequency dLOFC and dHOFC were also observed. All in all, individual-band and between-frequency tFC and dFC can provide complementary information to the traditional individual-band LOFC for assessing driving drowsiness.

References

[1] S. K. L. Lal and A. Craig, "A critical review of the psychophysiology of driver fatigue," *Biol. Psychol.*, vol. 55, no. 3, pp. 173–194, Feb. 2001.

[2] H. J. Eoh, M. K. Chung, and S.-H. Kim, "Electroencephalographic study of drowsiness in simulated driving with sleep deprivation," *Int. J. Ind. Ergonom.*, vol. 35, no. 4, pp. 307–320, Apr. 2005.

[3] S. M. Marcora, W. Staiano, and V. Manning, "Mental fatigue impairs physical performance in humans," *J. Appl. Physiol.*, vol. 106, no. 3, pp. 857–864, Mar. 2009.

[4] P. Thiffault and J. Bergeron, "Monotony of road environment and driver fatigue: A simulator study," *Accident Anal. Prevention*, vol. 35, no. 3, pp. 381–391, 2003.

[5] G. Zhang, K. K. Yau, X. Zhang, and Y. Li, "Traffic accidents involving fatigue driving and their extent of casualties," *Accident Anal., Prevention*, vol. 87, pp. 34–42, Feb. 2016.

[6] C. Zhao, M. Zhao, J. Liu, and C. Zheng, "Electroencephalogram and electrocardiograph assessment of mental fatigue in a driving simulator," *Accident Anal. Prevention*, vol. 45, pp. 83–90, Mar. 2012.

[7] S. K. L. Lal and A. Craig, "Driver fatigue: Electroencephalography and psychological assessment," *Psychophysiology*, vol. 39, no. 3, pp. 313–321, May 2002.

[8] G. Borghini, L. Astolfi, G. Vecchiato, D. Mattia, and F. Babiloni, "Measuring neurophysiological signals in aircraft pilots and car drivers for the assessment of mental workload, fatigue and drowsiness," *Neurosci. BioBehav. Rev.*, vol. 44, pp. 58–75, Jul. 2014.

[9] C. Papadelis *et al.*, "Monitoring sleepiness with on-board electrophysiological recordings for preventing sleep-deprived traffic accidents," *Clin. Neurophysiol.*, vol. 118, no. 9, pp. 1906–1922, 2007.

[10] J. Harvy, E. Sigalas, N. Thakor, A. Bezerianos, and J. Li, "Performance improvement of driving fatigue identification based on power spectra and connectivity using feature level and decision level fusions," in *Proc. 40th Annu. Int. Conf. IEEE Eng. Med. Biol. Soc. (EMBC)*, Jul. 2018, pp. 102–105.

[11] J. Hi *et al.*, "Boosting transfer learning improves performance of driving drowsiness classification using EEG," in *Proc. Int. Workshop Pattern Recognit. Neuroimag. (PRNI)*, Jun. 2018, pp. 1–4.

[12] M. Simon *et al.*, "EEG alpha spindle measures as indicators of driver fatigue under real traffic conditions," *Clin. Neurophysiol.*, vol. 122, no. 6, pp. 1168–1178, 2011.

[13] J. Perrier, S. Jongen, E. Vuurman, M. L. Bocca, J. G. Ramaekers, and A. Vermeeren, "Driving performance and EEG fluctuations during on-the-road driving following sleep deprivation," *Biol. Psychol.*, vol. 121, pp. 1–11, Dec. 2016.

[14] E. Wascher *et al.*, "Frontal theta activity reflects distinct aspects of mental fatigue," *Biol. Psychol.*, vol. 96, pp. 57–65, Feb. 2014.

[15] H. Wang, A. Dragomir, N. I. Abbasi, J. Li, N. V. Thakor, and A. Bezerianos, "A novel real-time driving fatigue detection system based on wireless dry EEG," *Cogn. Neurodyn.*, vol. 12, no. 4, pp. 365–376, Feb. 2018.

[16] W. Kong, Z. Zhou, B. Jiang, F. Babiloni, and G. Borghini, "Assessment of driving fatigue based on intra/inter-region phase synchronization," *Neurocomputing*, vol. 219, pp. 474–482, Jan. 2017.

[17] J. P. Liu, C. Zhang, and C. X. Zheng, "Estimation of the cortical functional connectivity by directed transfer function during mental fatigue," *Appl. Ergonom.*, vol. 42, no. 1, pp. 114–121, Dec. 2010.

[18] B. T. Jap, S. Lal, and P. Fischer, "Inter-hemispheric electroencephalography coherence analysis: Assessing brain activity during monotonous driving," *Int. J. Psychophysiol.*, vol. 76, no. 3, pp. 169–173, Jun. 2010.

[19] M. M. Lorist, E. Bezdan, C. M. Ten, M. M. Span, J. B. Roerdink, and N. M. Maurits, "The influence of mental fatigue and motivation on neural network dynamics; an EEG coherence study," *Brain Res.*, vol. 1270, pp. 95–106, May 2009.

[20] W. Kong, W. Lin, F. Babiloni, S. Hu, and G. Borghini, "Investigating driver fatigue versus alertness using the granger causality network," *Sensors*, vol. 15, no. 8, pp. 19181–19198, Aug. 2015.

[21] Y. Sun, J. Lim, K. Kwok, and A. Bezerianos, "Functional cortical connectivity analysis of mental fatigue unmasks hemispheric asymmetry and changes in small-world networks," *Brain Cogn.*, vol. 85, pp. 220–230, Mar. 2014.

[22] C. Zhang, X. Yu, Y. Yang, and L. Xu, "Phase synchronization and spectral coherence analysis of EEG activity during mental fatigue," *Clin. EEG Neurosci.*, vol. 45, no. 4, pp. 249–256, Oct. 2014.

[23] C. Zhao, M. Zhao, Y. Yang, J. Gao, N. Rao, and P. Lin, "The reorganization of human brain networks modulated by driving mental fatigue," *IEEE J. Biomed. Health Informat.*, vol. 21, no. 3, pp. 743–755, May 2017.

[24] J. Li *et al.*, "Mid-task break improves global integration of functional connectivity in lower alpha band," *Frontiers Hum. Neurosci.*, vol. 10, p. 304, Jun. 2016.

[25] M. D. Domenico, "Multilayer modeling and analysis of human brain networks," *Giga Sci.*, vol. 6, no. 5, pp. 1–8, May 2017.

[26] M. J. Brookes *et al.*, "A multi-layer network approach to MEG connectivity analysis," *NeuroImage*, vol. 132, pp. 425–438, May 2016.

[27] P. Tewarie *et al.*, "Integrating cross-frequency and within band functional networks in resting-state MEG: A multi-layer network approach," *NeuroImage*, vol. 142, pp. 324–336, Nov. 2016.

[28] X. Chen, H. Zhang, S. W. Lee, D. Shen, and A. D. N. Initiative, "Hierarchical high-order functional connectivity networks and selective feature fusion for MCI classification," *Neuroinformatics*, vol. 15, no. 3, pp. 271–284, Jul. 2017.

[29] H. Zhang, X. Chen, Y. Zhang, and D. Shen, "Test-retest reliability of 'high-order' functional connectivity in young healthy adults," *Frontiers Neurosci*, vol. 11, p. 439, Aug. 2017.

[30] X. Chen *et al.*, "High-order resting-state functional connectivity network for MCI classification," *Hum. Brain Mapping*, vol. 37, no. 9, pp. 3282–3296, Sep. 2016.

[31] Y. Zhang, H. Zhang, X. Chen, S.-W. Lee, and D. Shen, "Hybrid high-order functional connectivity networks using resting-state functional MRI for mild cognitive impairment diagnosis," *Sci. Rep.*, vol. 7, p. 6530, Jul. 2017.

[32] H. Zhang *et al.*, "Topographical information-based high-order functional connectivity and its application in abnormality detection for mild cognitive impairment," *J. Alzheimer's Disease*, vol. 54, no. 3, pp. 1095–1112, Oct. 2016.

[33] A. Delorme and S. Makeig, "EEGLAB: An open source toolbox for analysis of single-trial EEG dynamics including independent component analysis," *J. Neurosci. Methods*, vol. 134, no. 1, pp. 9–21, Mar. 2004.

[34] P. D. Meo, E. Ferrara, G. Fiumara, and A. Provetti, "Generalized Louvain method for community detection in large networks," in *Proc. 11th Int. Conf. Intell. Syst. Design Appl. (ISDA)*, Nov. 2011, pp. 88–93.